

RESEARCH ARTICLE | MAY 22 2025

Quantum phase synchronization revealing few-hundred femtosecond coherence in cryptophyte phycoerythrin 545 antenna from exciton–vibrational coupling

Special Collection: [David Jonas Festschrift](#)

Jiayu Wang ; Jiading Zou ; Zhanghe Zhen; Hanting Meng ; Guohong Liao ; Li Liu ; Zhuan Wang ; Hailong Chen ; Yang Pu  ; Yuxiang Weng  

 Check for updates

J. Chem. Phys. 162, 205101 (2025)

<https://doi.org/10.1063/5.0259190>



Articles You May Be Interested In

Oscillations of the total kinematic momentum vector for viscous fluid dynamics in pipes of arbitrary section

Physics of Fluids (August 2023)



The Journal of Chemical Physics
**Special Topics Open
for Submissions**

[Learn More](#)

Quantum phase synchronization revealing few-hundred femtosecond coherence in cryptophyte phycoerythrin 545 antenna from exciton–vibrational coupling

Cite as: J. Chem. Phys. 162, 205101 (2025); doi: 10.1063/5.0259190

Submitted: 18 January 2025 • Accepted: 5 May 2025 •

Published Online: 22 May 2025



View Online



Export Citation



CrossMark

Jiayu Wang,^{1,2} Jiading Zou,^{1,3} Zhanghe Zhen,¹ Hanting Meng,^{1,2} Guohong Liao,^{1,2} Li Liu,¹ Zhuan Wang,^{1,3} Hailong Chen,^{1,2,3} Yang Pu,^{4,a)} and Yuxiang Weng^{1,2,3,a)}

AFFILIATIONS

¹Laboratory of Soft Matter Physics, Institute of Physics, Chinese Academy of Sciences, Beijing 100190, People's Republic of China

²University of Chinese Academy of Sciences, Beijing 100049, People's Republic of China

³Songshan Lake Materials Laboratory, Dongguan 523808, Guangdong, People's Republic of China

⁴School of Fisheries, Ludong University, Yantai 264025, People's Republic of China

Note: This paper is part of the JCP Special Topic, David Jonas Festschrift.

^{a)}Authors to whom correspondence should be addressed: ypu@ldu.edu.cn and yxweng@iphy.ac.cn

ABSTRACT

Quantum beats lasting a few hundred femtoseconds have been regarded as signatures of quantum energy transfer in photosynthetic antennae. The fragile coherence at room temperature casts doubt on its long-lived feature arising from the electronic coherence. Recently, the long-lived exciton–vibrational coherences of several hundred femtoseconds via quantum phase synchronization of the resonant higher frequency collective vibrational modes have been observed in core antenna allophycocyanin from algae. The long-lived coherence has an inherent property of protecting the coherence against the noisy environment. This is achieved by dissipation of the resonant anti-symmetric collective vibrational modes coupled to the excitonic levels, which have fast dephasing, leaving only the non-dissipative correlated symmetric modes [R. Zhu *et al.*, Nat. Commun. 15, 3171 (2024)], which is different from that induced by the environmental low frequency modes. Coherence with a lifetime constant of 200 fs at room temperature has been observed in the cryptophyte phycoerythrin 545 (PE545) antenna before, while its origin, i.e., pure electronic or exciton–vibrational, remains to be explored. Here, we investigated coherent energy transfer dynamics in PE545 via two-dimensional electronic spectroscopy. A long-lasting coherence with a lifetime constant of 270 fs in the dynamical Stokes shift dynamics was observed. Especially, the high frequency vibrational mode at 1150 cm⁻¹ is absent in the electronic energy dissipation process reflected in the dynamical Stokes' shifts spectrum, which is near resonant with the electronic gap of 1080 cm⁻¹. Therefore, the facts strongly suggest that the long-lived coherence in PE545 is realized by the resonant exciton–vibrational coupling via quantum phase synchronization.

Published under an exclusive license by AIP Publishing. <https://doi.org/10.1063/5.0259190>

I. INTRODUCTION

Photosynthesis is one of the most efficient processes in nature through which solar energy is converted into chemical energy with quantum efficiency over 90%.¹ Its high efficiency has attracted considerable research interest for decades, especially benefiting from the maturation of ultrafast spectroscopy techniques with coherent excitation.^{2–5} Long-lasting coherence in spectroscopic signals

has been observed in various light-harvesting complexes at room temperature,^{6–8} and quantum coherent excitation energy transfer (EET) was proposed as a potential mechanism to account for the high efficiency in the ultrafast EET processes,^{9–12} in contrast to the Förster resonance energy transfer (FRET) mechanism.^{13,14} In the coherent EET mechanism, the excitation energy is instantaneously quantum-mechanically shared among several nearby interacting pigments and is transferred among pigments as wave packets,

which enables the protein–pigment complexes to find the most efficient EET path.^{15–17} Pure electronic coherence has been confirmed to be helpless to EET processes, owing to its short-lived lifetime (around 50 fs) at room temperature, incommensurable with the timescale of EET of several hundred fs to ps.¹⁸ Meanwhile, exciton–vibrational coherence originating from the interplay between electronic and nuclear degrees of freedom has been verified to accelerate the EET rate, i.e., the underdamped vibrations resonant with the exciton energy splitting known as the vibronic states delocalize across two or more pigment molecules.^{19–22} Dephasing occurs when the coherent superposition states are subject to random environmental perturbations, especially the broad homogeneous spectral lines of light-harvesting complexes indicative of strong chromophore–environment interactions, where pure electronic state coherence can only last for a very limited timespan at room temperature, typically tens of fs.^{23,24} At 77 K in the Fenna–Matthews–Olson (FMO) complex, where the timescale for electronic energy transfer is about 350 fs, the experimentally determined electronic dephasing time is 240 fs, the decay time for the excited-state vibronic coherence is 570 fs, while the dephasing time for ground-state vibrational coherence is about 2 ps.²⁴ As it has been explained by Christensson *et al.*, for the strongly coupled system, the long-lived coherences in FMO are based on coherent superpositions of vibronic exciton states with dominant vibrational contributions from excitations on the same pigment.²⁵ Though further experimental and theoretical verification are still needed, the first trial to isolate the excited state vibronic coherence shows that inter-exciton coherence has a sub-100 fs dephasing time in a homodimer of biscyanine at an ambient temperature,²⁶ while other coherent exciton–vibrational (vibronic) couplings as the origin of long-lasting coherence in artificial light harvesters have also been reported.^{27–29} However, the origin of the long-lasting coherence is still a matter of ongoing debate, as it is unclear how the light-harvesting systems suppress the loss of coherence due to interaction with the noisy environments to sustain a long-lasting coherence.^{18,30}

The synchronous behavior in the system–bath coupling is important for the survival of quantum correlations and entanglement in the quantum system.³¹ It has been suggested that spatially correlated environmental fluctuations might support the long-lasting coherent dynamics of electronic excitations.^{32,33} By coupling between the bath modes of low frequencies of two distinct excitons, correlated spectral motion would occur in the electronic states, preserving their phase relationships longer.³² However, atomistic descriptions have challenged the idea of spatially correlated fluctuations in FMO complexes.³⁴ Since this proposal emphasizes the correlated motion of the environment, it can be regarded as passive synchronization. Later theoretical studies combining classical molecular dynamics (MD) and quantum chemical methods indicated that spatial correlations did not translate into significant correlations among the site energies in FMO and phycoerythrin 545 (PE545).^{35–37} It has also been hypothesized that some energy is reversibly transferred between the chromophores and environmental bath modes throughout the transport process, leading to reversible, oscillatory energy transfer among excited states.³⁸

Although the correlated site energy fluctuations for the protein-bound pigments were proposed for the observed long-lasting coherence, it has been disproved by subsequent simulations; therefore, it is challenging to identify any such “protection” of coherences.²⁴

Theoretical studies have focused on the other coherence-protection mechanisms, i.e., transient synchronization in exciton–vibrational coupled systems as vibronic dimers.^{31,39,40} In this model, the localized intramolecular vibrational coordinates can be projected into symmetric and antisymmetric vibrational coordinates, and only the antisymmetric vibrations can be coupled to the excitonic levels. Tiwari *et al.* pointed out that it was the anti-correlated component of the vibrations that coupled to the electronic state that induced the energy gap fluctuation, which in turn drove energy transfer through nonadiabatic dynamics.⁴¹ The results of these studies have shown that coherent energy transport is concomitant with the emergence of positive synchronization (in phase) between mode displacements, which suggests that coherence in pigments promotes the synchronization of vibrational motions driven by thermal equilibrium or environmental noise. Moreover, transient spontaneous synchronization can lead to very weak energy dissipation due to collective motion,^{31,39,42} therefore, the synchronization is believed to be driven by the environmental noise or the low frequency modes of the correlated motions of the proteins that bind the pigments.⁴³ It has long been known that correlated vibrations that are delocalized across pigments oscillate coherently throughout the process of energy transfer between the pigments, as observed experimentally.^{43,44} In addition, it is explained in a dimer model in which each chromophore supports a single vibrational mode, showing that when coherence transfer to the acceptor occurs, the coherence trapping in the donor can increase the longevity of vibronic quantum beats beyond the time scale for electronic energy exchange.⁴⁵

In our recent work on the exciton–vibrational model, Weng *et al.* showed that the synchronization between the anti-symmetric and symmetric collective modes of higher frequency modes for an excitonic dimer was actively initiated by the dissipation of the resonant anti-symmetric modes by the coupled delocalized excitonic states with fast dephasing, leaving only non-dissipative symmetric collective modes.⁴² Generally, when the electronic gap energy is larger than $k_B T$ (200 cm^{-1}), synchronization occurs without the participation of the environmental noise of slower motion.⁴² The predicted half loss in coherent Raman intensity of the resonant modes in a strongly coupled system, non-dissipation of the resonant modes in dynamical Stokes shift spectra, and long-lasting coherence have been experimentally confirmed in the allophycocyanin (APC) trimer. It is expected that this predicted phenomenon based on the quantum phase synchronization in the excitonic–vibrational mode can be a consensus to examine the origin of long-lasting coherence in other photosynthetic antenna systems, i.e., pure electronic, vibrational, or excitonic–vibrational.

We want to extend the above consensus to the other light-harvesting complex, which can be a potential candidate of an electronic–vibrational coupling system for the observed long-lasting coherence. PE545 is the only type of phycobiliprotein in cryptophyte algae of the *Rhodomonas*, in which PE545 acts as the major light-harvesting antenna.^{46,47} Cryptophyte is one of the most primitive photosynthetic organisms, surviving under relatively poor lighting conditions in the ocean and utilizing the sunlight more efficiently than terrestrial plants.⁴⁸ Therefore, the EET pathways in PE545 have been investigated intensively both in theory and experiments.^{49–51} Figure 1(a) represents the crystal structure of PE545 with resolution up to 1.10 \AA (PDB ID code 1XF6), which consists of four polypeptide chains, including two α subunits (labeled as A and B)

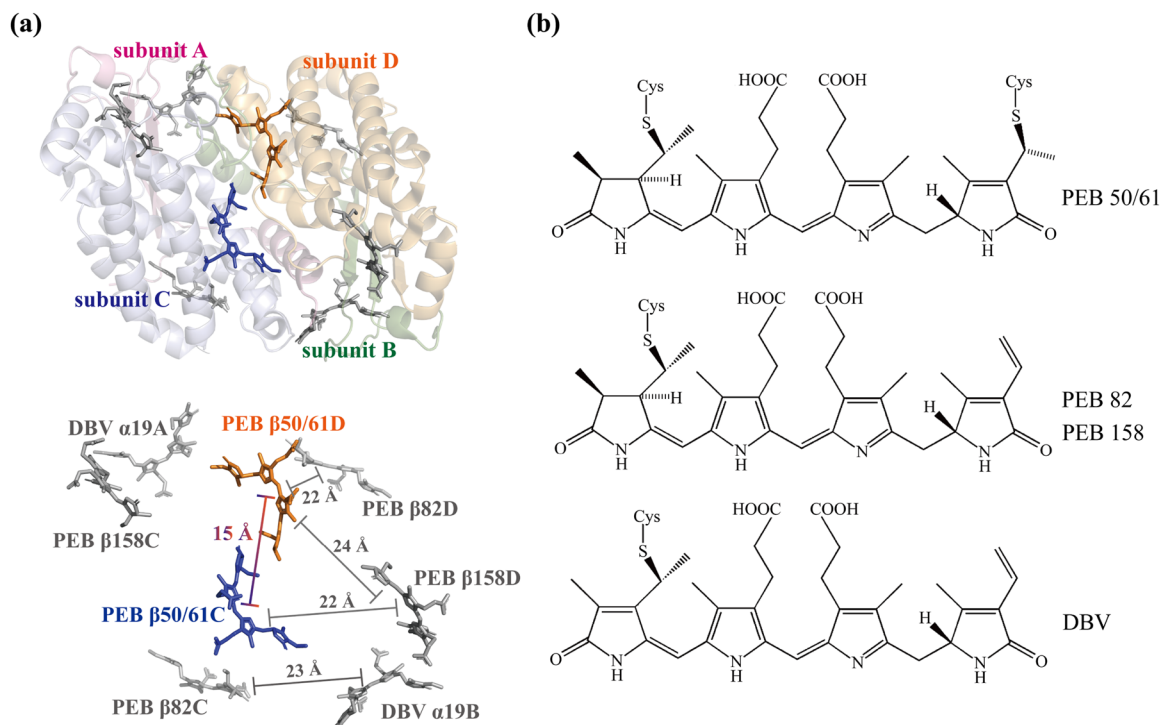


FIG. 1. (a) Top: The x-ray structure of the dimeric PE545 from cryptomonad *Rhodomonas* CS24 (PDB ID code 1XF6) with the four protein subunits (A–D) shown in pink (α), green (α), blue (β), and orange (β). Bottom: The distribution of the pigments in PE545 with the distances between them. The coupled pigment pairs PEB β 50/61C and PEB β 50/61D with the shortest distance of 15 Å are plotted in blue and orange. (b) The chemical structures of the phycoerythrobilin (PEB) and dihydrobiliverdin (DBV) pigments. The structure of PEB β 50/61 is plotted in the top panel, that of PEB β 82 and PEB β 158 is in the middle panel, and that of DBV is in the bottom panel.

and two β subunits (labeled as C and D), arranged in a dimeric complex of $\alpha\beta$ monomers. There are eight pigment molecules inside the PE545 dimer, and all the pigments are covalently bound to the protein frame. A monomer contains three phycoerythrobilin (PEB 50/61, PEB 158, and PEB 82) pigments in the β subunit and one dihydrobiliverdin (DBV 19) pigment in the α subunit. The chemical structures of these pigments are plotted in Fig. 1(b). The closest pigments in the PE545 dimer, between PEB 50/61C and PEB 50/61D across the monomer-monomer interface, are separated by a center-to-center distance of 15 Å,⁵² forming an excitonic dimer of the strongest coupling. The difference CD spectrum between the dimer and monomer shown in Fig. S5 exhibits a typical excitonic feature of PE545 with a fitted coupling constant of 276 cm^{-1} , a value larger than the earlier calculated one of 248 cm^{-1} and the later calculated one of 92 cm^{-1} .^{51,52} In the PE545 monomer, there are two pigment pairs with weak electronic coupling, i.e., between DBV 19B and PEB 82C (45 cm^{-1}) and between DBV A and PEB 82D (46 cm^{-1}).⁵¹ These two pigment pairs also have weak electronic coupling (33–40 cm^{-1}) with PEB 50/61C and PEB 50/61D, respectively. The coupling constant derived from CD measurements is larger than those of calculations; this is possibly owing to contributions from the other more weakly coupled pairs. Therefore, the calculated value of 92 cm^{-1} is used as the coupling constant for the PEB 50/61C-PEB 50/61D dimer. Long-lived quantum coherence lasting at least 200 fs has been observed by means of 2DES at room temperature.^{6,53,54}

The observed oscillations were assigned to the electronic rather than the vibrational coherences,⁵⁴ while this slow dephasing of electronic coherence was suggested to be due to the presence of shared or correlated motions in the surrounding environment.⁶ In addition, the covalent attachment of the chromophores to their protein environment was thus believed to support or strengthen correlated motions between chromophores and protein.⁶ Viani *et al.* analyzed the degree of correlated fluctuations in the PE545 by combining MD simulations with quantum mechanics/molecular mechanics calculations and showed that the effect of fluctuations and correlations in site energies on the observed long-lived coherences was almost negligible in the PE545.³⁵ On the other hand, Kolli *et al.* investigated the role of high-energy quantized vibrations that were quasi-resonant with excitonic transitions in non-equilibrium dynamics for energy transfer.³⁷ Their results showed that the beating pattern of excitonic coherences in the presence of these vibrations had a dual origin, i.e., short-time oscillations lasting for about 50–100 fs from pure electronic coherence and a superimposed vibration-induced modulation that survived close to the picosecond timescale. Therefore, the origin of the long-lasting coherence in PE545 is still controversial.

In this work, we utilize 2DES and heterodyne-detected transient grating (HD-TG) and broadband transient absorption (BBTA) to investigate the EET processes and coherence dynamics in PE545. Compared to the APC trimer, which contains three identical pairs of α 84– β 84 excitonic dimers, PE545 consists of only one pair of

relatively stronger coupled excitonic dimers of PEB 50/61C-PEB 50/61D among a total of eight pigment molecules. This results in a congested absorption spectrum, making it more challenging to identify the potential electronic–vibrational coherence in PE545. We directly resolved the ultrafast EET process within the PEB 50/61 pigment pair with a lifetime constant of 50 fs. By monitoring the excited-state resolved dynamical Stokes shift, we found a 270-fs coherence lifetime in the dimer, which is more than twofold of the coherence lifetime observed in the monomer (120 fs). Furthermore, the excitonic–vibrational mode at 1150 cm^{-1} shows zero amplitude in the corresponding dynamical Stokes shift spectrum at the lower energy level of the excitonic dimer, indicating that this mode is not involved in the electronic energy dissipation process of the dimer. In addition, double-cross (DC) polarization-controlled HD-TG measurements further reveal that the mode at 1150 cm^{-1} originates from excitonic–vibrational coherence. Therefore, we conclude that quantum phase synchronization is realized for the resonant collective mode of 1150 cm^{-1} in PE545, and this mode is attributed to the resonance excitonic–vibrational coherence mode responsible for the observed long-lasting quantum coherence in the excitonic dimer.

II. METHOD

A. Sample preparation

The analytical grade PE545 ($\text{Abs}_{545}/\text{Abs}_{280} = 10$) was purified from unicellular cryptophyte algae of the *Rhodomonas salina*. The purification process of PE545 is briefly described as follows:^{55–57} this marine cryptophyte strain preserved in our laboratory was cultured at 20°C in f/2 artificial seawater culture media. After 20 days, through centrifugation (4000 rpm, 10 min, 4°C), the algae biomass was separated from the culture medium and then stored at -80°C . The stored algal cells were mixed with a 0.02M phosphate buffer solution (pH 6.9) at a mass-to-volume ratio of 1:10. Upon completing three freeze–thaw cycles, centrifugation (12 000 rpm, 30 min, 4°C) was performed to obtain PE545-enriched supernatant. Then, the supernatant was treated with 50% (w/v) saturated ammonium sulfate to precipitate impurity. After centrifugation (12 000 rpm, 20 min, 4°C), the supernatant solution containing PE545 was filtered through a $0.22\text{ }\mu\text{m}$ cellulose acetate membrane for subsequent purification with fast protein liquid chromatography (FPLC). The FPLC device equipped with a Butyl-S Sepharose 6 Fast Flow column was then used to obtain the final analytical grade PE545 through gradient elution with the various concentrations of $(\text{NH}_4)_2\text{SO}_4$. Following SDS-PAGE, three bands at the expected positions (α_1 and α_2 subunits around 10 kDa and the β subunit around 20 kDa) were confirmed by Coomassie Brilliant Blue staining (Fig. S1 in the supplementary material). In addition, according to the different retention times, PE545 dimer and PE545 monomer were separated (Fig. S2 in the supplementary material) in gel filtration chromatography (Superdex-200 Increase 10/300 GL, GE, USA).

B. Spectroscopy

The principle of 2DES and the setup used for the experiments have been described in detail elsewhere, while a brief description is given here.^{58–60} In the 2DES experiment, a sequence of three

identical ultrashort laser pulses excites the sample to induce a four-wave mixing (FWM) signal, which interferes with another pulse (local oscillator, LO). From the heterodyne interference signal, we could obtain both the intensity and the phase of the FWM signal. After Fourier transform (FT), a 3D array comprising excitation frequency, emission frequency, and waiting time is obtained, from which both the spectral evolution of the system and the quantum coherence beating signals can be extracted. The setup used for 2DES experiments comprises a home-built non-collinear optical parametric amplifier (NOPA) and a non-collinear BOXCARs 2DES setup with an angle between the beam pairs of 2.6° . The pulses with a spectrum centered at 550 nm were compressed to 9 fs (Fig. S3 of the supplementary material) using a combination of a grating pair and a fused silica prism pair. The coherence time (τ) between the first two pulses was scanned by a 1.35-fs step from -54 to 54 fs. The waiting time (T) of 2DES was scanned by an 8-fs step within a temporal region of 1 ps and then scanned at uneven intervals to 100 ps. An excitation energy of 1 nJ per pulse was used for all measurements with the spot size ($100 \times 100\text{ }\mu\text{m}^2$) at the sample. The excitation energy density was $\sim 12\text{ }\mu\text{J}/\text{cm}^2$. 2DES data were averaged over ten times in two independent experiments to obtain a higher quality of coherent dynamics. The polarization combination involved in the all-parallel (AP) 2DES and HD-TG experiments is $(0^\circ, 0^\circ, 0^\circ, 0^\circ)$, while that for the DC HD-TG experiment is $(45^\circ, -45^\circ, 90^\circ, 0^\circ)$.

III. RESULTS AND DISCUSSION

A. Quantum phase synchronization via resonant exciton–vibrational coupling of the collective modes

The observed long-lived coherence has been explained by a model of resonant exciton–vibrational coupling of the collective mode to a dimeric exciton, as illustrated in Fig. 2, exemplified with an interacting PEB 50/61D and PEB 50/61C pigment pair in PE545 is plotted, where two PEB pigments form a non-degenerate homodimer, and each molecule possesses an identical intramolecular harmonic vibration with a frequency of ω in resonance with the excitonic energy gap ΔE . The corresponding Hamiltonian,

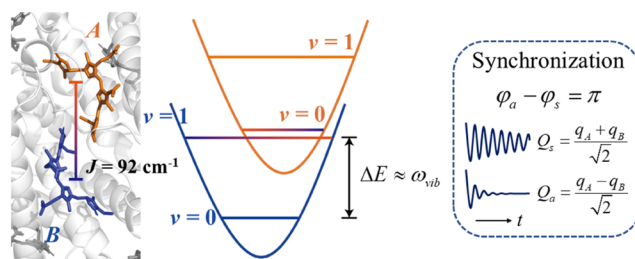


FIG. 2. Left: The energy diagram of the exciton–vibrational PEB 50/61 pigment dimer. PEB 50/61D and PEB 50/61C are labeled as molecules A and B, respectively. Right: q_A and q_B are localized intramolecular vibrational coordinates. The anti-symmetric (Q_a) modes undergo fast energy dissipation via coupling of the delocalized excitonic levels, and the symmetric (Q_s) modes survive. Correction: We fix the error in Fig. 5(c) in reprinted with permission from Zhu *et al.*, Nat. Commun. **15**, 3171 (2024). Copyright 2024 Springer Nature, where Q_a and Q_s should be swapped.

including the ground state and two singly excited states (excitonic levels), is given by

$$\begin{aligned} \hat{H} = & T + [V_A(q_A) + V_B(q_B)]|g\rangle\langle g| \\ & + [\varepsilon_A + V_A(q_A^*) + V_B(q_B)]|e_1\rangle\langle e_1| \\ & + [\varepsilon_A + V_A(q_A) + V_B(q_B^*)]|e_2\rangle\langle e_2| \\ & + J[|e_1\rangle\langle e_2| + |e_2\rangle\langle e_1|], \end{aligned} \quad (1)$$

where T is the kinetic energy, $V(q)$ is the potential energy surface, q^* and q are the dimensionless coordinates of the excited and ground states for the two molecules, respectively, and they satisfy the equation of $q_i^* = q_i + d_i$, where d_i is the dimensionless displacement of nuclear coordinate for the excited state with respect to that of the ground state. $|g\rangle$ and $|e\rangle$ represent the ground and excited states on a local electronic wave function basis, respectively. The intramolecular vibrational modes are converted into two intermolecular collective modes, i.e., the symmetric collective component, $Q_s = (q_A + q_B)/\sqrt{2}$, and the anti-symmetric collective component, $Q_{as} = (q_A - q_B)/\sqrt{2}$. Under weak electronic coupling (J) and a significant site energy difference ($\Delta = \varepsilon_A - \varepsilon_B$), i.e., $\Delta/2 \gg J$, the eigenenergies of the two delocalized states can be derived as follows:

$$\begin{aligned} E_+ &= (\varepsilon_A + \hbar\omega S) + \frac{1}{2}\hbar\omega(Q_s^{*2} + Q_a^{*2}) - \hbar\omega\sqrt{S}(Q_s^* - Q_a^*), \\ E_- &= (\varepsilon_B + \hbar\omega S) + \frac{1}{2}\hbar\omega(Q_s^{*2} + Q_a^{*2}) - \hbar\omega\sqrt{S}(Q_s^* + Q_a^*), \end{aligned} \quad (2)$$

where the subscripts \pm indicate the upper and lower energy levels, respectively.

Apparently, the electronic energy without the contribution of the pure vibrational energy can be expressed as

$$\begin{aligned} E_+ &= (\varepsilon_A + \hbar\omega S) - \hbar\omega\sqrt{S}(Q_s^* - Q_a^*), \\ E_- &= (\varepsilon_B + \hbar\omega S) - \hbar\omega\sqrt{S}(Q_s^* + Q_a^*). \end{aligned} \quad (3)$$

After impulsive optical excitation, vibrational wave packets are created in both the excited state and the ground state, and the intramolecular vibrational mode experiences a Brownian force from the environment and undergoes underdamped oscillation.⁶¹ Such underdamped oscillation would appear as oscillation in the population dynamics and modulates the energy levels of the excited states temporarily.⁶² Under the assumption that Gaussian stochastic random force due to solvent motion acting on the j th vibrational mode takes on zero, the nuclear motion for the j th underdamped oscillation can be derived as

$$q(t) = A_0 e^{-\frac{\gamma_j t}{2}} \left(\cos(\bar{\omega}_j t + \varphi_j) + \frac{\gamma_j}{2\bar{\omega}_j} \sin(\bar{\omega}_j t + \varphi_j) \right), \quad (4)$$

where φ is the initial phase and A_0 is the oscillation amplitude, γ is the relaxation rate, and $\bar{\omega}_j = [\omega_j^2 - (\gamma_j/2)^2]^{1/2}$. For the vibrational modes of high-frequencies, such as $>500 \text{ cm}^{-1}$, $\gamma \ll \omega_j$, and we have $\bar{\omega}_j \approx \omega_j$; therefore,

$$q(t) \approx A e^{-\frac{\gamma_j t}{2}} \left(\cos(\omega_j t + \varphi_j) + \frac{\gamma_j}{2\omega_j} \sin(\omega_j t + \varphi_j) \right). \quad (5)$$

The excited state nuclear motion $q^*(t)$ takes the same form as that of $q(t)$, while the parameters such as A , γ , and φ can be different. When a dimer is considered, Eq. (5) also applies to the motion of the collective modes. The detailed derivation of Eq. (4) can be found in Sec. 12.3 of the [supplementary material](#).⁴²

In the measurement of the time-dependent dynamical Stokes shift, generally the upper excitonic level (E_+) decays too fast to be measured; we focus only on the lower energy level (E_-), i.e., and the time-dependent term is

$$E_-(t) = -\hbar\omega\sqrt{S}(Q_s^*(t) + Q_a^*(t)). \quad (6)$$

In a weakly coupled excitonic dimer, taking the relaxation rates for the asymmetric and symmetric collective modes as $\gamma_s \approx \gamma_{as}$, we substitute the motion equation for the j th collective mode described by Eq. (5) into Eq. (6), the time-dependent dynamical Stokes shift of the lower excitonic energy level coupled to the j th vibrational mode is given as

$$\begin{aligned} E_-^j(t) &= -2A_0^* \sqrt{S_j} \hbar\omega_j e^{-\frac{\gamma_j^* t}{2}} \cos\left(\frac{\varphi_s^j - \varphi_a^j}{2}\right) \\ &\times \left[\cos\left(\omega_j t + \frac{\varphi_s^j + \varphi_a^j}{2}\right) + \frac{\gamma_j^*}{2\omega_j} \sin\left(\omega_j t + \frac{\varphi_s^j + \varphi_a^j}{2}\right) \right], \end{aligned} \quad (7)$$

where φ_s^j and φ_{as}^j are the initial phases of the symmetric and anti-symmetric collective modes, which can be uncorrelated initially in a weakly coupled dimer. In Eq. (7), if the anti-symmetric and symmetric collective modes are synchronized, i.e., $\varphi_s^j - \varphi_{as}^j = \pi$,³¹ then we have $E_-^j(t) = 0$, which indicates that the synchronized vibrational modes would not participate in the electronic energy dissipation.

We then show that for the resonant modes in a strongly coupled system, the phase synchronization can be realized by the following mechanism. By using the Hamiltonian for the delocalized excitonic basis, the local electronic wave function basis is changed to the delocalized excitonic basis ($|E_i\rangle$) via a rotation operator $U(\theta)$,³¹

$$\begin{pmatrix} |E_1\rangle \\ |E_2\rangle \end{pmatrix} = U^\dagger(\theta) \begin{pmatrix} |e_1\rangle \\ |e_2\rangle \end{pmatrix}, \quad (8)$$

where $U(\theta) = \begin{pmatrix} \cos \theta & \sin \theta \\ -\sin \theta & \cos \theta \end{pmatrix}$. $\theta = \frac{1}{2} \arctan\left(\frac{2J}{\Delta}\right)$ is referred to as the mixing angle, which is an effective measure of the delocalization of the electronic sub-system or the exciton size. $\Delta = \varepsilon_A - \varepsilon_B$ is the site energy difference. Subsequently, the exciton-vibrational coupling Hamiltonian is

$$H_{\text{coupling}} = \hbar\omega\sqrt{S} \sin(2\theta) Q_a^* \sigma_x, \quad (9)$$

where $\sigma_x = |E_1\rangle\langle E_2| + |E_2\rangle\langle E_1|$ is the transition operator. Obviously, for strongly coupled systems, only the anti-symmetric collective modes can be coupled to the two delocalized excitonic states. Therefore, once the anti-symmetric collective modes are in resonance with the two delocalized excitonic states, vibrational energy will be dissipated to the environment through fast excitonic dephasing (30 fs^{-1}), leaving only the correlated symmetric collective modes surviving, i.e., $\gamma_{as} \gg \gamma_s$. This automatically leads to the correlated motion of the two molecules after a certain period of time, even though the

initial phases can be different. Since the resonant symmetric collective modes are decoupled to the excitonic states, they do not participate in the electronic energy dissipation process, which renders the excitonic dimer an active mechanism of protecting the vibrational coherence against the environmental fluctuations.

As a result, for either the weakly coupled ($\gamma_{as} \approx \gamma_s$) or strongly coupled systems ($\gamma_{as} \gg \gamma_s$), the resonant vibrational mode would not appear in the dynamical Stokes shift spectra. This provides three experimentally measurable consensus for verification of the observed long-lasting coherence as the excitonic–vibrational coherence in origin:

- (1) Half-loss in Raman intensity for the near resonant coherent vibrational modes in a strongly coupled excitonic pair in contrast to the Raman intensity of the corresponding modes in the isolated molecules.

In the experimental measurement of the coherences, the Raman intensity of the vibrational modes is measured by Fourier transformation of the oscillation kinetics; therefore, the intensity (I) of the given mode can be deduced as inversely proportional to its relaxation rate (k), i.e., $\frac{I_{as}}{I_s} = \frac{k_s}{k_{as}}$. Taking the relation rate of the anti-symmetric mode of fast relaxation as that of the electronic dephasing rate $k_{as} = 1/50 \text{ fs}^{-1}$ and $k_s = 1/1000 \text{ fs}^{-1}$, we have $\frac{I_{as}}{I_s} = 0.05 \approx 0$; therefore, the Raman intensity of the coherent mode at the excited states in a strongly coupled dimer is almost equal to that of the symmetric collective mode, i.e., $I_s^* = I_{iso}^*$, which is half of the intensity for two isolated molecules ($2I_{iso}^*$), where I_{iso}^* denotes the Raman intensity of an excited isolated molecule (Sec. 12 in the [supplementary material](#)). As to the Raman intensity for the mode at the ground state, *Tivari et al.* have shown that during the resonance Raman excitation of the strongly coupled dimer, anti-correlated vibrational wave packets are in resonance with the electronic transition.⁴¹ Therefore, the anti-correlated collective modes are dominant in the ground state. As a result, for a strongly coupled dimer, a loss in Raman intensity for the near-resonant coherent vibrational modes in the ground state is expected.

The half-loss in Raman intensity for strongly coupled dimers has also been proposed by *Tiwari and Jonas* before in terms of Huang–Rhys factors for the collective modes.⁶³ The Huang–Rhys factor of the correlated vibration (S_j^+) is half of that for the isolated pigment mode ($S_j^+ = \frac{1}{2}S_{iso}$), while the Huang–Rhys factor of the anti-correlated vibration (S_j^-) is equal to or less than half of that for the isolated pigment vibration ($S_j^- = \frac{\cos^2(2\theta_d)}{2}S_{iso}$), where θ_d is the excitonic mixing angle and defined by $2\theta_d = \arctan(\frac{2J}{\Delta})$. The sum of S_j^+ and S_j^- is greater than or equal to $S_j^+ = \frac{1}{2}S_{iso}$, becoming equal for strong coupling (complete excitonic delocalization). This sum is also less than or equal to S_{iso} , becoming equal in the absence of excitonic mixing.

- (2) Absence of the near resonant vibrational modes in the dynamical Stokes shift coherence spectra for both weakly and strongly coupled systems.
- (3) Longer coherence lifetime in the exciton than that in the non-excitonic system.

All these three consensus have been verified in a relatively strongly coupled APC consisting of three identical excitonic pairs. As shown in [Fig. 1](#), PE545 only has one excitonic pair in the presence of six other monomeric pigments with severely congested absorption spectra; therefore, it is challenging to inspect the origin of the long-lasting coherence in PE545.

B. 2DES spectra and the amplitudes of resonant vibrational modes in the coherence spectra

The absorption and fluorescence spectra of the PE545 dimer are shown in [Fig. 3](#) (blue and red lines) and can be covered by the broadband spectra of the excitation pulses for the 2DES measurement (the shaded area in [Fig. 3](#)). The reported energy positions of 8 exciton states ($k = 1$ –8) are plotted as vertical sticks in [Fig. 3](#); their assignments to the respective pigments are given in [Table S1](#), while the simulated absorption spectra of the excitons are plotted in [Fig. S6](#). Specifically, the states $k = 1$ at $\omega_1 = 19120 \text{ cm}^{-1}$ (orange stick) and $k = 5$ at $\omega_1 = 18040 \text{ cm}^{-1}$ (blue stick) correspond to the exciton levels of the PEB 50/61D–PEB 50/61C dimer, with an energy splitting of around 1080 cm^{-1} . The site energy difference between the excitonic dimers is estimated to be 1042 cm^{-1} .⁵¹ PE545 belongs to a weakly coupled system ($\frac{2J}{\Delta E} = 0.17$) in the diabatic pigment basis.⁶⁴ The absorption and fluorescence spectra of the PE545 monomer are shown in [Fig. S4](#) in the [supplementary material](#) for comparison.

[Figure 4\(a\)](#) presents the pure absorptive 2DES of the PE545 dimer at $T = 24$ and 200 fs and 2 and 100 ps . The positive peaks elongated along the diagonal are assigned to ground-state bleaching (GSB) and stimulated emission (SE) signals of the PEB and DBV pigments. EET processes among the pigments in PE545 are clearly shown by the spectral evolution over time, i.e., the increased amplitude of the cross peak below the diagonal and the concomitant decrease of the diagonal peak in the 2D maps. The grid shown by gray dotted lines in [Fig. 4\(a\)](#) highlights the positions of the energy levels for the PEB 50/61D–PEB 50/61C excitonic pair in the

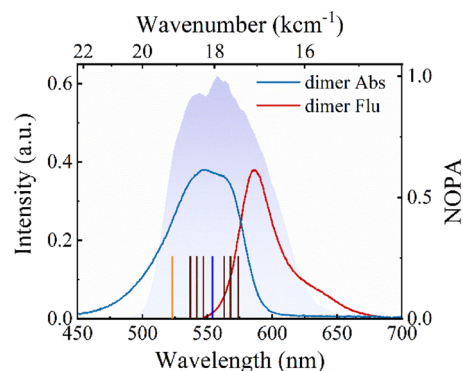


FIG. 3. Absorption spectrum (blue) and fluorescence spectrum (red) of PE545 at room temperature and the broadband spectral profile of the excitation laser pulses used in 2DES measurements (shaded in purple). The vertical sticks indicate the exciton levels fitted by spectral simulation. The exciton levels of PEB 50/61D and PEB 50/61C are highlighted in orange sticks and blue sticks, respectively. The sticks are reprinted with permission from *Novoderezhkin et al.*, *Biophys. J.* **99**, 344 (2010). Copyright 2010 Elsevier.

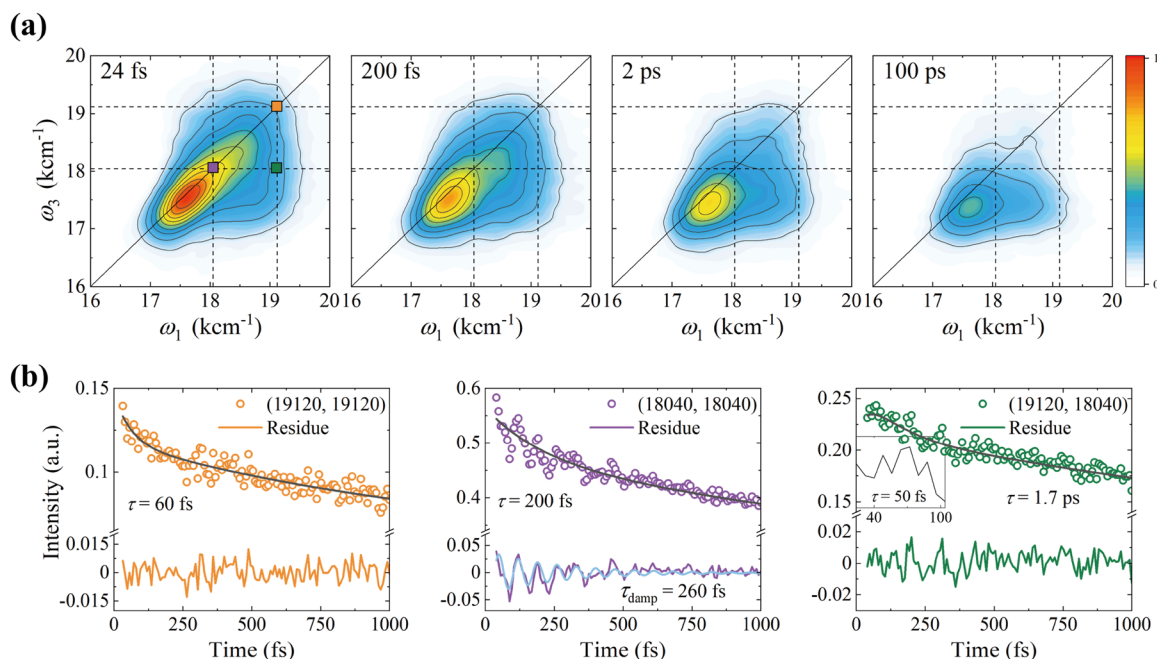


FIG. 4. (a) Pure absorptive 2D maps of PE545 recorded at the waiting times of $T = 24, 200$ fs, 2 , and 100 ps with dashed lines indicating the excitonic energy levels. (b) The population relaxation dynamics from 40 fs to 1 ps at the diagonal peaks at $(19\ 120, 19\ 120)$ cm^{-1} and $(18\ 040, 18\ 040)$ cm^{-1} and the energy transfer dynamics at the cross peak at $(19\ 120, 18\ 040)$ cm^{-1} . The raw data are shown in dots, and the fitting results using multi-exponential function $f(t) = \sum_{i=1}^4 A_i \exp(-t/\tau_i)$ are shown in black lines, where τ is the lifetime constant and A is the corresponding coefficient. The graphic inset in $(19\ 120, 18\ 040)$ cm^{-1} enlarges the component indicative of rising from 24 to 104 fs. The color in the legend of (b) corresponds to the peak positions marked with squares of the same color as (a).

2D spectra. The dynamics of the two excitonic levels at the two diagonal peaks of $(19\ 120, 19\ 120)$ cm^{-1} and $(18\ 040, 18\ 040)$ cm^{-1} have respective decay time constants of 60 and 200 fs, while the cross peak at $(19\ 120, 18\ 040)$ cm^{-1} indicative of energy transfer from the upper excitonic level to the lower one, shows a slight increase in the amplitude at the early stage [see the inset in Fig. 4(b), right panel], subsequent with a slower relaxation process, aligning with the simulated pure electronic dephasing time of about 50 fs in the PEB excitonic pair at room temperature.³⁷ The weak rise in the dynamics could be attributed to the interference of pulse overlapping effects in the early stage, and the more weighted decay component originated from the energy relaxation of PEB 50/61C. We also inspected the energy transfer dynamics at another predicted cross peak at $(18\ 340, 17\ 620)$ cm^{-1} , which represents the EET process from the higher 545 nm energy band to the lower 567 nm energy band. As shown in Fig. S7, the fitting results reveal a EET process with a lifetime constant of 780 fs, corresponding to the EET process from the central PEB 50/61D-PEB 50/61C dimer to the four peripheral pigments, i.e., PEB 158 and PEB 82, which are consistent with the literature values.⁵¹ The pure absorptive 2DES of PE545 monomer is shown in Fig. S8 in the [supplementary material](#). The spectral features of the 2D maps of dimer and monomer are nearly the same. The EET dynamics of the PE545 monomer are shown in Fig. S11. The slow processes on the picosecond timescale at the cross peak $(18\ 340, 17\ 620)$ cm^{-1} fall in the incoherent Förster EET mechanism regime. Therefore, the

influence of the weak electronic coupling among pigments in the monomer could be ignored in our following discussion.

In addition, we have observed clear quantum beats at the lower excitonic level at $(18\ 040, 18\ 040)$ cm^{-1} , shown as the residuals in Fig. 4(b), middle panel. The oscillation amplitude is nearly 5% of the population, which has a decay time of 260 fs (damped oscillation fitting in the blue line), and is thus regarded as long-lasting coherence. After subtracting the fitted decay envelopes, we could observe abundant oscillatory features in both PE545 dimer and monomer, especially within the first 1 ps time window, as shown in Figs. 4(b) and S11. We performed Fourier transformation on the oscillatory residual from 40 fs to 1 ps and then integrated the coherent amplitude across the 2D spectra for both the dimer and the monomer. Nine significant coherent frequencies at $210, 370, 500, 870, 1150, 1230, 1360, 1588,$ and 1630 cm^{-1} were observed in the coherent spectra for both the dimer and the monomer, as shown in Fig. 5(a). In particular, the blue-shaded region and blue line highlight the vibrational mode at 1150 cm^{-1} , which is assigned to the C-C and C-N stretching coupled to N-H and C-H rocking.⁶⁵ This mode is in the region of near-resonance with the excitonic energy splitting (1080 cm^{-1}) of the PEB 50/61D-PEB 50/61C pigment dimer. The BBTA experiments also revealed similar coherence information [see Fig. 5(b)]. Pre-resonant impulsive Raman HD-TG experiments (detailed in Sec. 8 in the [supplementary material](#)) were performed to characterize the Raman modes as shown in Fig. 5(c). These

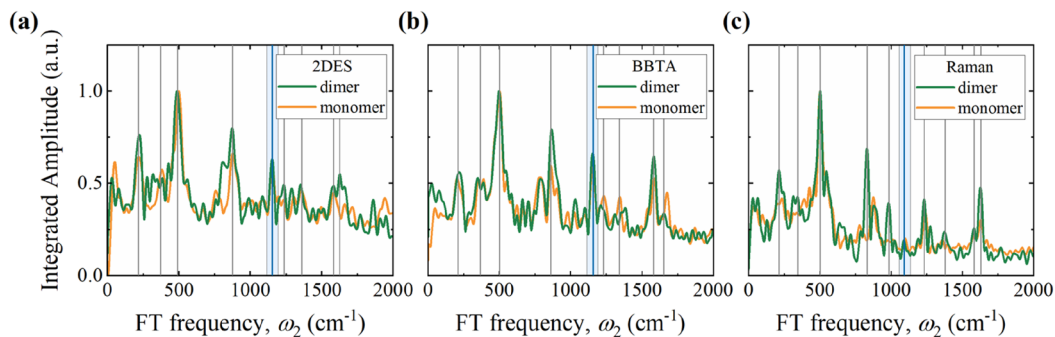


FIG. 5. Integrated coherence spectra of PE545 dimer (green) and monomer (orange) from 2DES (a), BBTA (b), and impulsive Raman (c) by pre-resonant HD-TG measurements. The gray lines indicate vibrational modes at 210, 370, 500, 880, 1230, 1360, 1588, and 1630 cm^{-1} . The blue line and blue-shaded area highlight the vibrational mode at 1150 cm^{-1} . All spectra were normalized to the amplitude at 500 cm^{-1} . The spectra of NOPA used for impulsive Raman experiments and BBTA are plotted in Figs. S14 and S16.

frequencies are consistent with the reported vibrational frequencies of PE545, while the extra mode at 980 cm^{-1} comes from buffer, and the mode at 1150 cm^{-1} undergoes a red shift to 1090 cm^{-1} .^{37,66} A comparison of the coherent spectra of the dimer with that of the monomer revealed similar amplitude at 1150 cm^{-1} . The expected reduction in the amplitude of the resonant mode of 1150 cm^{-1} is much less compared to our previous report on APC, in which the resonant modes have a nearly 50% reduction in the vibrational amplitudes in the trimer than that in the α -subunit. The observed almost same Raman intensities in the PE545 dimer and monomer can be accounted for from two aspects. First, the weakly coupled nature of PE545 leads to a significantly smaller reduction in the Raman intensity of the resonant mode compared to the half-loss expected for strongly coupled systems.⁶³ Second, the PE545 contains six PEBs and two DBVs, but only two of the PEBs form the electronically coupled pigment pair, while the Raman intensities for every individual PEB and DBV molecule can be varied.³⁶ Therefore, unlike those in APC, half loss in the coherent Raman intensity cannot be observed in PE545.

The FT coherence maps (Fig. S19 in the [supplementary material](#)) from the 2D rephasing spectra of PE545 dimer and monomer exhibit similar characteristics, two broad peaks located on the upper cross peak and the lower cross peak, respectively. The pattern of the FT coherence maps depends on the origin of the coherence. Typically, pure electronic coherence distributes on the symmetric off-diagonal peaks, while the pure vibrational coherence in a displaced harmonic oscillator (DHO) system exhibits as a chair pattern.⁶⁷ The FT coherence map of exciton-vibrational coherence was predicted to exhibit an asymmetric enhanced amplitude at the lower cross peaks, which is attributed to the enhancement of delocalized and anticorrelated ground state wave packet excited via nonadiabatic excitonic-vibrational coupling.⁴¹ As shown in Fig. S19 in the [supplementary material](#), nearly all the FT coherence maps of PE545 exhibit an asymmetric intensity enhancement in the lower cross peak. We attributed this phenomenon to the fact that the ground state wave packets dominate the coherence signals under our excitation conditions.⁶⁸ Therefore, the ground-state amplitude enhancement in the FT coherence maps cannot serve as a criterion for the excitonic-vibronic coupling in PE545.

C. Excited state resolved dynamical Stokes shift spectra

Apart from the spectral evolution originating from EET, the diagonal peaks undergo spectral broadening along the anti-diagonal direction and redshift along the emission frequency due to energy relaxation of the excited electronic states through vibrational modes and solvent reorganization. These phenomena are known as solvation, which originates from the system-bath interaction.⁶⁹ The ultrafast solvation dynamics of electronically excited states can be revealed by the dynamical Stokes shift function $S(t)$, which is analogous to the frequency fluctuation correlation function in the linear response region.^{70,71} $S(t)$ was extracted from the 2D spectra by monitoring the shift of the diagonal peak along emission frequency as a function of waiting time (T). $S(t)$ extracted from the sliced spectra at $\omega_1 = 18\,040$ are shown in Fig. 6 (left panel), which corresponds to the lower excitonic states in the PEB 50/61D-PEB 50/61C dimer. $S(t)$ of the monomer extracted from BBTA measurement is shown in Fig. 6 (right panel).

As demonstrated in Fig. 6, dynamical Stokes shift decays with the increasing waiting time. We discerned two lifetime constants for the dimer and monomer by employing the sum of a Gaussian and a single-exponential decay function [$f(t) = A_d \exp[-t^2/(2\tau_d^2)] + A_e \exp(-t/\tau_e) + C$] from 40 fs to 1 ps. The fitting results are listed in Table S2 in the [supplementary material](#). In the dimer, the ultrafast process with a lifetime constant of 66 fs is dominated by the inertial solvent response, and the slower process with a lifetime constant of 550 fs is dominated by the subsequent diffusive response. In the monomer, the two lifetime constants are 47 fs and 1.6 ps, respectively. The former accounts for a significant portion of the equilibration process and is governed by the solvent dynamics, while the latter, over a time scale comparable to that of the energy transfer (1 ps), aligns with findings from previous studies on similar proteins.⁷¹ The residuals of the dynamical Stokes shift are plotted in the lower panel, respectively. The oscillations originate from the coherent coupling of vibrational modes to electronic states as wave packets, which are created by the excitation of an ultrashort light pulse with a broad spectral bandwidth. The accurate coherent lifetime constants of the wavepackets are hard to be accurately determined because of the superposition of

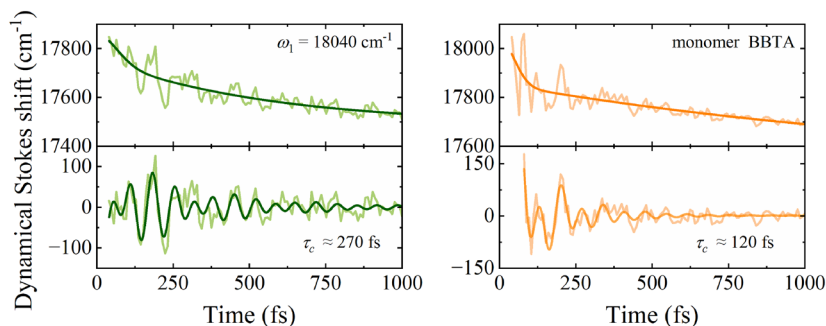


FIG. 6. 2DES-detected dynamical Stokes shift of PE545 dimer at $\omega_1 = 18040 \text{ cm}^{-1}$ (the lower excitonic level in PEB 50/61D-PEB 50/61C pigment pair) and the BBTA-detected dynamical Stokes shift of PE545 monomer. The energy relaxation kinetics are fitted with the sum of a Gaussian and single exponential decay function from 40 fs to 1 ps. The oscillatory residual curves are plotted in the bottom panel, with the fitting results with damped oscillation function from 40 to 1 ps for 2DES and from 80 fs to 1 ps for BBTA to avoid the jitter arising from the interference between the probe and the scattering light of the pump.

multiple vibrational modes, while the envelopes of the residues reveal a longer coherent lifetime in the exciton–vibrational coupled pigments dimer than that in the monomer. The coherence lifetime constants are fitted by $f(t) = A_{e1} \exp(-t/\tau_{e1}) \sin(2\pi\omega_1 \cdot t + \phi_1) + A_{e2} \exp(-t/\tau_{e2}) \sin(2\pi\omega_2 \cdot t + \phi_2) + C$. The estimated average lifetime constants (τ_c) for the wave packets are ~ 270 fs for the dimer and ~ 120 fs for the monomer. The fitting results are detailed in Table S3 in the [supplementary material](#).

The dynamical Stokes shift coherence spectra of the dimer from 2DES measurements were derived through Fourier transformation of the corresponding oscillatory residual curve of $S(t)$ and

are shown in [Fig. 7\(a\)](#). The spectra were averaged at several nearby spectral slices to increase the signal-to-noise ratio. In the dimer, the near-resonant mode at 1150 cm^{-1} disappears in the FT spectrum from the dynamical Stokes shift at the spectral slices at $\omega_1 = 17980\text{--}18080 \text{ cm}^{-1}$, corresponding to the lower excitonic states of the PEB 50/61D-50/61C pigment pair. In contrast, the mode appears in the other spectral slices from $\omega_1 = 17700\text{--}17800 \text{ cm}^{-1}$ and $\omega_1 = 17360\text{--}17460 \text{ cm}^{-1}$, corresponding to the energy levels of PEB 82C and DBV A, respectively. As shown in the amplitude profile of the mode at 1150 cm^{-1} along excitation frequency (ω_1) from pure absorptive 2DES [[Fig. 7\(b\)](#)], the mode mainly distributes at around

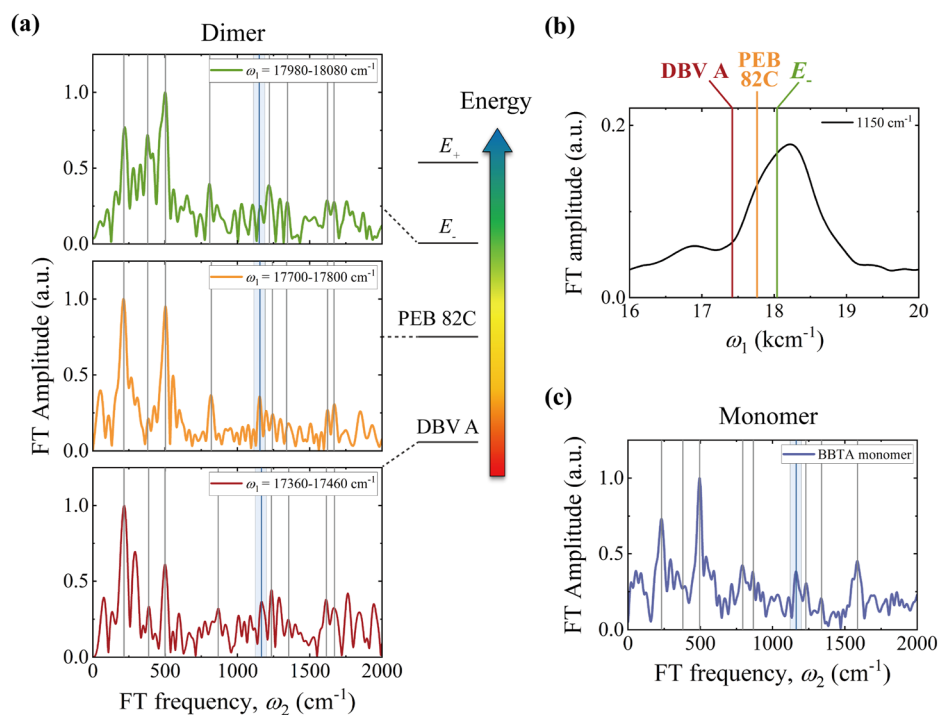


FIG. 7. (a) Excited-state resolved dynamical Stokes shift coherence spectra from 40 fs to 1 ps of PE545 dimer at $\omega_1 = 17980\text{--}18080 \text{ cm}^{-1}$ (top), $\omega_1 = 17700\text{--}17800 \text{ cm}^{-1}$ (middle), $\omega_1 = 17360\text{--}17460 \text{ cm}^{-1}$ (bottom), corresponding to the lower excitonic level of the PEB 50/61D-50/61C pigments pair, PEB 82C, and DBV A, respectively. The resonant mode at 1150 cm^{-1} is highlighted by a blue line, which is absent in the coherence spectrum at $\omega_1 = 17980\text{--}18080 \text{ cm}^{-1}$ but appears in other spectra. (b) Intensity distribution of the 1150 cm^{-1} mode along excitation frequency ω_1 (integrated over the emission frequency ω_3) from pure absorptive 2DES of PE545 dimer. (c) Dynamical Stokes shift coherence spectra from 80 fs to 1 ps of PE545 monomer from BBTA measurements.

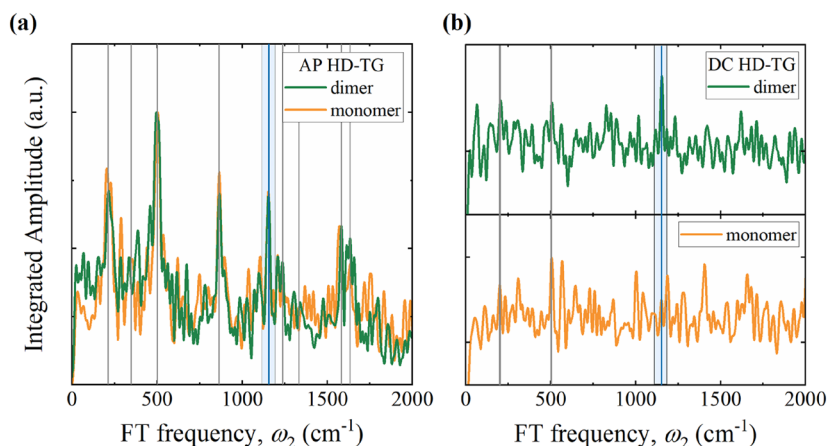


FIG. 8. Comparison of the FT spectra of the PE545 dimer (green) and monomer (orange) from AP HD-TG (a) and DC HD-TG (b) measurements. The blue shaded area highlights the mode at 1150 cm^{-1} .

$\omega_1 = 17980\text{--}18080\text{ cm}^{-1}$ and has relatively small amplitudes at $\omega_1 = 17700\text{--}17800\text{ cm}^{-1}$ and $\omega_1 = 17360\text{--}17460\text{ cm}^{-1}$, indicating that the near-resonant modes are strongly suppressed only in the coherence spectra of dynamical Stokes shift at the lower excitonic states in the coupled pigment pair. In addition, the dynamical Stokes shift coherence spectrum of the PE545 monomer from BBTA is plotted in Fig. 7(c) with the presence of the vibrational mode at 1150 cm^{-1} .

Furthermore, DC HD-TG experiments were performed for both PE545 dimer and monomer, as detailed in Sec. 8 in the supplementary material. The polarization combination of $(45^\circ, -45^\circ, 90^\circ, 0^\circ)$ is effective to distinguish electronic coherence as well as excitonic-vibrational coherence from vibrational coherence by suppressing the latter with respect to the AP HD-TG $(0^\circ, 0^\circ, 0^\circ, 0^\circ)$.²⁴ For the population state signals in AP HD-TG and DC HD-TG, a suppression ratio of about 75 was achieved. As shown in the FT spectra for the PE545 dimer from DC HD-TG [green line in Fig. 8(b)], two intense modes at 210 and 500 cm^{-1} still appear. However, the intensity of the 1150 cm^{-1} mode is significantly enhanced compared to that in AP HD-TG [Fig. 8(a)]. In contrast, in the monomer, all the modes, including 1150 cm^{-1} are suppressed in DC HD-TG (orange line in Fig. 8). Therefore, we attribute the origin of the mode at 1150 cm^{-1} in the PE545 dimer to excitonic-vibrational coherence, consistent with the conclusion derived from the dynamical Stokes shift analysis.

The dynamical Stokes shift characterizes the dissipation of the excited-state energy, and its oscillatory behavior can be assigned to intramolecular vibrational modes. Therefore, the coherence

spectrum of dynamical Stokes shift can be used to characterize the intramolecular or solvent vibrational modes participating in the electronic energy dissipation processes. Our results suggest that the exciton-vibrational modes in the dimer do not participate in the electronic energy dissipation process; therefore, the exciton-vibrational coherence of the excitonic dimer in the PE545 dimer is protected against fluctuating environmental noise, which accounts for the longer coherence time. These results validate the prediction from the quantum phase synchronization of the resonant collective mode in the excitonic dimer, where the absence of the near resonant vibrational modes in the dynamical Stokes shift coherence spectra is expected. Therefore, based on our results, the consensus for experimental identification of the electronic-vibrational coupling can be summarized in Table I.

IV. CONCLUSION

We found the ultrafast EET process with a lifetime constant of 50 fs within the PEB 50/61 pigment pair in PE545. Abundant oscillatory signals were revealed, and the near-resonant mode at 1150 cm^{-1} is attributed to exciton-vibrational coherence. By monitoring dynamical Stokes shift, the coherence lifetime constant of the dimer was estimated to be around 270 fs, much longer than that of 120 fs in the monomer. The near-resonant mode is absent in the dynamical Stokes shift at the lower excitonic state of the PEB 50/61D-50/61C pigment dimer and is therefore hardly involved in the energy dissipation process. Our results validated the predictions from the quantum phase synchronization mechanism, which suggests that anti-symmetric resonant collective vibrational modes coupled with electronic states undergo fast dephasing and reveal the phase synchronization with the long-lived symmetric collective modes. In addition to APC, PE545 provides another example of the quantum phase synchronization mechanism for suppressing the environmental fluctuations in a biological system, which leads to a long-lasting excitonic-vibrational coherence.

Exciton-vibrational coherence and quantum phase synchronization can be a general strategy for protection of the long-lasting coherence in the excitonic dimer within the light-harvesting systems. It serves as a quantum analog of the classical Huygens synchronization of two pendulum clocks,^{72,73} where either anti-phase

TABLE I. Consensus for experimental identification of electronic-vibrational coupling.

Consensus	Weakly coupled	Strongly coupled
Absence of coherent modes in dynamical Stokes shift spectrum	Yes	Yes
Half-loss in Raman intensity	No	Yes
Longer coherence time than isolated molecule	Yes	Yes

or in-phase oscillations can survive from the initial two oscillations depending on the construction of the pendulum clocks, i.e., for the anti-phase motion, the two identical pendulum clocks are weakly coupled through a heavy beam, while for in-phase motion, the ratio of the beam frequency to the pendulum frequency is very small, or the damping of the beam is not too large, and the maximum amplitude of the oscillators is sufficiently small.⁷⁴

SUPPLEMENTARY MATERIAL

See the [supplementary material](#) for additional sample preparation analysis, pulse characterization, circular dichroism spectrum, supplementary 2D spectra, energy transfer dynamics, supplementary analysis of BBTA and HD-TG, dynamical Stokes shift, FT coherence maps, and time-frequency analysis.

ACKNOWLEDGMENTS

This work was financially supported by the National Natural Science Foundation of China (Grant Nos. T2350011, 22027802, and 22222308) and the Natural Science Foundation of Shandong Province (Grant No. ZR2021LLZ003).

AUTHOR DECLARATIONS

Conflict of Interest

The authors have no conflicts to disclose.

Author Contributions

J.W. and J.Z. contributed equally to this work.

Jiayu Wang: Data curation (lead); Formal analysis (lead); Investigation (lead); Methodology (equal); Visualization (lead); Writing – original draft (lead). **Jiading Zou:** Data curation (lead); Formal analysis (lead); Methodology (lead). **Zhanghe Zhen:** Resources (lead). **Hanting Meng:** Data curation (supporting). **Guohong Liao:** Formal analysis (supporting). **Li Liu:** Methodology (supporting). **Zhuan Wang:** Investigation (supporting); Methodology (supporting). **Hailong Chen:** Investigation (supporting); Methodology (supporting). **Yang Pu:** Investigation (supporting); Resources (lead); Supervision (lead). **Yuxiang Weng:** Conceptualization (lead); Formal analysis (lead); Methodology (lead); Supervision (lead); Writing – original draft (lead).

DATA AVAILABILITY

The data that support the findings of this study are available from the corresponding authors upon reasonable request.

REFERENCES

- ¹R. E. Blankenship, 2002.
- ²T. Brixner, J. Stenger, H. M. Vaswani, M. Cho, R. E. Blankenship, and G. R. Fleming, *Nature* **434**, 625 (2005).
- ³M. D. Edington, R. E. Riter, and W. F. Beck, *J. Phys. Chem.* **100**, 14206 (1996).

- ⁴G. D. Scholes, *J. Phys. Chem. Lett.* **1**, 2 (2010).
- ⁵F. D. Fuller and J. P. Ogilvie, *Annu. Rev. Phys. Chem.* **66**, 667 (2015).
- ⁶E. Collini, C. Y. Wong, K. E. Wilk, P. M. G. Curmi, P. Brumer, and G. D. Scholes, *Nature* **463**, 644 (2010).
- ⁷J. M. Womick, B. A. West, N. F. Scherer, and A. M. Moran, *J. Phys. B: At., Mol. Opt. Phys.* **45**, 154016 (2012).
- ⁸J. M. Womick and A. M. Moran, *J. Phys. Chem. B* **113**, 15747 (2009).
- ⁹P. Bhattacharyya and G. R. Fleming, *J. Chem. Phys.* **153**, 044119 (2020).
- ¹⁰E. A. Arsenaault, Y. Yoneda, M. Iwai, K. K. Niyogi, and G. R. Fleming, *Nat. Commun.* **11**, 1460 (2020).
- ¹¹J. S. Higgins, M. A. Allodi, L. T. Lloyd, J. P. Otto, S. H. Sohail, R. G. Saer, R. E. Wood, S. C. Massey, P.-C. Ting, R. E. Blankenship, and G. S. Engel, *Proc. Natl. Acad. Sci. U. S. A.* **118**, e2018240118 (2021).
- ¹²E. J. O'Reilly and A. Olaya-Castro, *Nat. Commun.* **5**, 3012 (2014).
- ¹³Th. Förster, "Intermolecular energy migration and fluorescence," *Ann. Phys.* **437**(1-2), 55–75 (1948).
- ¹⁴G. D. Scholes, *Annu. Rev. Phys. Chem.* **54**, 57 (2003).
- ¹⁵E. Collini, *Chem. Soc. Rev.* **42**, 4932 (2013).
- ¹⁶G. S. Engel, T. R. Calhoun, E. L. Read, T.-K. Ahn, T. Mančal, Y.-C. Cheng, R. E. Blankenship, and G. R. Fleming, *Nature* **446**, 782 (2007).
- ¹⁷A. Chenu and G. D. Scholes, *Annu. Rev. Phys. Chem.* **66**, 69 (2015).
- ¹⁸H.-G. Duan, V. I. Prokhorenko, R. J. Cogdell, K. Ashraf, A. L. Stevens, M. Thorwart, and R. J. D. Miller, *Proc. Natl. Acad. Sci. U. S. A.* **114**, 8493 (2017).
- ¹⁹S. Polyutov, O. Kühn, and T. Pullerits, *Chem. Phys.* **394**, 21 (2012).
- ²⁰F. D. Fuller, J. Pan, A. Gelzinis, V. Butkus, S. S. Senlik, D. E. Wilcox, C. F. Yocum, L. Valkunas, D. Abramavicius, and J. P. Ogilvie, *Nat. Chem.* **6**, 706 (2014).
- ²¹J. M. Womick and A. M. Moran, *J. Phys. Chem. B* **115**, 1347 (2011).
- ²²P. Lei, J. Cheng, C. Zhang, W. Zhang, H. He, and X. Leng, *J. Chem. Phys.* **162**, 055101 (2025).
- ²³S. Mukamel, *Principles of Nonlinear Optical Spectroscopy* (Oxford University Press, New York, 1995).
- ²⁴E. Thyryhaug, R. Tempelaar, M. J. P. Alcocer, K. Židek, D. Bina, J. Knoester, T. L. C. Jansen, and D. Zigmantas, *Nat. Chem.* **10**, 780 (2018).
- ²⁵N. Christensson, H. F. Kauffmann, T. Pullerits, and T. Mančal, *J. Phys. Chem. B* **116**, 7449 (2012).
- ²⁶A. Halpin, P. J. M. Johnson, R. Tempelaar, R. S. Murphy, J. Knoester, T. L. C. Jansen, and R. J. D. Miller, *Nat. Chem.* **6**, 196 (2014).
- ²⁷J. Lim, D. Paleček, F. Caycedo-Soler, C. N. Lincoln, J. Prior, H. von Berlepsch, S. F. Huelga, M. B. Plenio, D. Zigmantas, and J. Hauer, *Nat. Commun.* **6**, 7755 (2015).
- ²⁸L. Wang, G. B. Griffin, A. Zhang, F. Zhai, N. E. Williams, R. F. Jordan, and G. S. Engel, *Nat. Chem.* **9**, 219 (2017).
- ²⁹S. H. Sohail, J. P. Otto, P. D. Cunningham, Y. C. Kim, R. E. Wood, M. A. Allodi, J. S. Higgins, J. S. Melinger, and G. S. Engel, *Chem. Sci.* **11**, 8546 (2020).
- ³⁰H.-G. Duan, A. Jha, L. Chen, V. Tiwari, R. J. Cogdell, K. Ashraf, V. I. Prokhorenko, M. Thorwart, and R. J. D. Miller, *Proc. Natl. Acad. Sci. U. S. A.* **119**, e2212630119 (2022).
- ³¹S. Siwiak-Jaszek, T. P. Le, and A. Olaya-Castro, *Phys. Rev. A* **102**, 032414 (2020).
- ³²B. S. Rolczynski, H. Zheng, V. P. Singh, P. Navotnaya, A. R. Ginzburg, J. R. Caram, K. Ashraf, A. T. Gardiner, S.-H. Yeh, S. Kais, R. J. Cogdell, and G. S. Engel, *Chem* **4**, 138 (2018).
- ³³H. Lee, Y.-C. Cheng, and G. R. Fleming, *Science* **316**, 1462 (2007).
- ³⁴C. Olbrich, J. Strümpfer, K. Schulten, and U. Kleinekathöfer, *J. Phys. Chem. B* **115**, 758 (2011).
- ³⁵L. Viani, C. Curutchet, and B. Mennucci, *J. Phys. Chem. Lett.* **4**, 372 (2013).
- ³⁶L. Viani, M. Corbella, C. Curutchet, E. J. O'Reilly, A. Olaya-Castro, and B. Mennucci, *Phys. Chem. Chem. Phys.* **16**, 16302 (2014).
- ³⁷A. Kolli, E. J. O'Reilly, G. D. Scholes, and A. Olaya-Castro, *J. Chem. Phys.* **137**, 174109 (2012).
- ³⁸G. Panitchayangkoon, D. V. Voronine, D. Abramavicius, J. R. Caram, N. H. C. Lewis, S. Mukamel, and G. S. Engel, *Proc. Natl. Acad. Sci. U. S. A.* **108**, 20908 (2011).
- ³⁹S. Siwiak-Jaszek and A. Olaya-Castro, *Faraday Discuss.* **216**, 38 (2019).
- ⁴⁰K. H. Cho and Y. M. Rhee, *J. Phys. Chem. B* **125**, 5601 (2021).

- ⁴¹V. Tiwari, W. K. Peters, and D. M. Jonas, *Proc. Natl. Acad. Sci. U. S. A.* **110**, 1203 (2013).
- ⁴²R. Zhu, W. Li, Z. Zhen, J. Zou, G. Liao, J. Wang, Z. Wang, H. Chen, S. Qin, and Y. Weng, *Nat. Commun.* **15**, 3171 (2024).
- ⁴³M. H. Vos, F. Rappaport, J.-C. Lambry, J. Breton, and J.-L. Martin, *Nature* **363**, 320 (1993).
- ⁴⁴S. E. Bradforth, R. Jimenez, F. van Mourik, R. van Grondelle, and G. R. Fleming, *J. Phys. Chem.* **99**, 16179 (1995).
- ⁴⁵J. A. Cina and G. R. Fleming, *J. Phys. Chem. A* **108**, 11196 (2004).
- ⁴⁶R. Maccoll, D. Guard-Friar, and E. C. Williams, *J. Lumin.* **51**, 21 (1992).
- ⁴⁷K. E. Wilk, S. J. Harrop, L. Jankova, D. Edler, G. Keenan, F. Sharples, R. G. Hiller, and P. M. G. Curmi, *Proc. Natl. Acad. Sci. U. S. A.* **96**, 8901 (1999).
- ⁴⁸H. W. Rathbone, K. A. Michie, M. J. Landsberg, B. R. Green, and P. M. G. Curmi, *Nat. Commun.* **12**, 1890 (2021).
- ⁴⁹A. B. Doust, C. N. J. Marai, S. J. Harrop, K. E. Wilk, P. M. G. Curmi, and G. D. Scholes, *J. Mol. Biol.* **344**, 135 (2004).
- ⁵⁰A. B. Doust, I. H. M. van Stokkum, D. S. Larsen, K. E. Wilk, P. M. G. Curmi, R. van Grondelle, and G. D. Scholes, *J. Phys. Chem. B* **109**, 14219 (2005).
- ⁵¹V. I. Novoderezhkin, A. B. Doust, C. Curutchet, G. D. Scholes, and R. van Grondelle, *Biophys. J.* **99**, 344 (2010).
- ⁵²A. B. Doust, K. E. Wilk, P. M. G. Curmi, and G. D. Scholes, *J. Photochem. Photobiol., A* **184**, 1 (2006).
- ⁵³D. B. Turner, K. E. Wilk, P. M. G. Curmi, and G. D. Scholes, *J. Phys. Chem. Lett.* **2**, 1904 (2011).
- ⁵⁴C. Y. Wong, R. M. Alvey, D. B. Turner, K. E. Wilk, D. A. Bryant, P. M. G. Curmi, R. J. Silbey, and G. D. Scholes, *Nat. Chem.* **4**, 396 (2012).
- ⁵⁵M. J. Broughton, C. J. Howe, and R. G. Hiller, *Gene* **369**, 72 (2006).
- ⁵⁶S. Zauner, T. Heimerl, D. Moog, and U. G. Maier, *Genome Biol. Evol.* **11**, 1618 (2019).
- ⁵⁷Y. Pu, S. Dong, J. Wang, M. Li, K. Dong, W. Li, and Z. Tang, *Protein Expression Purif.* **227**, 106634 (2025).
- ⁵⁸R. Zhu, S. Yue, H. Li, X. Leng, Z. Wang, H. Chen, and Y. Weng, *Opt. Express* **27**, 15474 (2019).
- ⁵⁹J. Zou, R. Zhu, J. Wang, H. Meng, Z. Wang, H. Chen, and Y.-X. Weng, *J. Phys. Chem. Lett.* **14**, 4657 (2023).
- ⁶⁰Y.-x. Weng, *Chin. J. Chem. Phys.* **31**, 135 (2018).
- ⁶¹Y. J. Yan and S. Mukamel, *Phys. Rev. A* **41**, 6485 (1990).
- ⁶²X.-Y. Cui, Y.-J. Yan, and J.-H. Wei, *Chin. Phys. B* **31**, 018201 (2022).
- ⁶³V. Tiwari and D. M. Jonas, *J. Chem. Phys.* **148**, 084308 (2018).
- ⁶⁴S. R.-K. Rodriguez, *Eur. J. Phys.* **37**, 025802 (2016).
- ⁶⁵F. Andel, J. T. Murphy, J. A. Haas, M. T. Mcdowell, I. van der Hoef, J. Lugtenburg, J. C. Lagarias, and R. A. Mathies, *Biochemistry* **39**, 2667 (2000).
- ⁶⁶A. J. Laos, J. C. Dean, Z. S. D. Toa, K. E. Wilk, G. D. Scholes, P. M. G. Curmi, and P. Thordarson, *Angew. Chem., Int. Ed.* **56**, 8384 (2017).
- ⁶⁷V. Butkus, D. Zigmantas, L. Valkunas, and D. Abramavicius, *Chem. Phys. Lett.* **545**, 40 (2012).
- ⁶⁸J. Wang, R. Zhu, J. Zou, H. Liu, H. Meng, Z. Zhen, W. Li, Z. Wang, H. Chen, Y. Pu, and Y. Weng, *J. Chem. Phys.* **161**, 085101 (2024).
- ⁶⁹G. R. Fleming and M. Cho, *Annu. Rev. Phys. Chem.* **47**, 109 (1996).
- ⁷⁰J. Lu, Y. Lee, and J. M. Anna, *J. Phys. Chem. B* **124**, 8857 (2020).
- ⁷¹C. C. Jumper, P. C. Arpin, D. B. Turner, S. D. McClure, S. R. Rather, J. C. Dean, J. A. Cina, P. A. Kovac, T. Mirkovic, and G. D. Scholes, *J. Phys. Chem. Lett.* **7**, 4722 (2016).
- ⁷²B. Tyagi, H. Li, E. R. Bittner, A. Piryatinski, and C. Silva-Acuña, *J. Phys. Chem. Lett.* **15**, 10896 (2024).
- ⁷³E. R. Bittner and B. Tyagi, *J. Chem. Phys.* **162**, 104116 (2025).
- ⁷⁴A. R. Willms, P. M. Kitanov, and W. F. Langford, *R. Soc. Open Sci.* **4**, 170777 (2017).